Atmos. Meas. Tech. Discuss., 6, 7315–7353, 2013
www.atmos-meas-tech-discuss.net/6/7315/2013/
doi:10.5194/amtd-6-7315-2013

Atmospheric Measurement Techniques Discussions

Impact of radar data assimilation using WRF three-dimensional variational system, for the simulation of a heavy rainfall case in Central Italy

I. Maiello[1], R. Ferretti[1], S. Gentile[1], M. Montopoli[2,3], E. Picciotti[4], F. S. Marzano[5], and C. Faccani[6]

[1]Centre of Excellence CETEMPS-Department of Physics, University of L'Aquila, L'Aquila, Italy
[2]University of Cambridge (UK), Dept. of Geography, Downing place CB4 3EN, Cambridge, UK
[3]Centre of Excellence CETEMPS-Department of Physics, University of L'Aquila, L'Aquila, Italy
[4]HIMET s.r.l., L'Aquila, Italy
[5]CETEMPS/Department of Information Engineering, Sapienza University of Rome, Rome, Italy
[6]ENAV S.p.A. – Academy, Forlì, Italy

Received: 15 March 2013 – Accepted: 30 July 2013 – Published: 8 August 2013

Correspondence to: I. Maiello (delfida2003@yahoo.it)

Published by Copernicus Publications on behalf of the European Geosciences Union.

Abstract

This work is a first assessment of the role of Doppler Weather radar (DWR) data in a mesoscale model for the prediction of a heavy rainfall. The study analyzes the event occurred during 19–22 May 2008 in the urban area of Rome. The impact of the radar reflectivity and radial velocity acquired from Monte Midia Doppler radar, on the assimilation into the Weather Research Forecasting (WRF) model version 3.2, is discussed. The goal is to improve the WRF high resolution initial condition by assimilating DWR data and using ECMWF analyses as First Guess thus improving the forecast of surface rainfall.

Several experiments are performed using different set of Initial Conditions (ECMWF analyses and warm start or cycling) and a different assimilation strategy (3 h-data assimilation cycle). In addition, 3DVAR (three-dimensional variational) sensitivity tests to outer loops are performed for each of the previous experiment to include the non-linearity in the observation operators.

In order to identify the best ICs, statistical indicators such as forecast accuracy, frequency bias, false alarm rate and equitable threat score for the accumulated precipitation are used. The results show that the assimilation of DWR data has a positive impact on the prediction of the heavy rainfall of this event, both assimilating reflectivity and radial velocity, together with conventional observations. Finally, warm start results in more accurate experiments as well as the outer loops strategy.

1 Introduction

The quality of the Initial Conditions is the most important parameter for the high resolution numerical weather prediction. Generally, localized mesoscale features are not well reproduced into the analysis therefore, assimilation approaches that ingest local observations are important to improve the forecast. During the last decade, high-resolution mesoscale models initialized using variational data assimilation techniques

AMTD
6, 7315–7353, 2013

(3DVAR/4DVAR) are being increasingly applied for studying meteorological phenomena (Kalnay, 2003). One of the reasons for the variational analysis becoming more and more popular is the ability to directly incorporate non conventional data such as satellite radiance, radar reflectivity and radial velocity into numerical models (Kalnay, 2003; Barker et al., 2004).

Doppler Weather radar (DWR) observations are an important data source for weather analyses and forecasting because of the high temporal and spatial resolutions. These high-resolution data, together with a sophisticated technique of data assimilation and a high-resolution mesoscale model, have been chosen in the last decade for improving the predictability both of convective cells and mesoscale convective systems. Furthermore, the assimilation of radar reflectivity and radial velocity have shown potential for very-short-range numerical prediction of rapidly developing convective systems. It is well known that the reflectivity is related to the amount of precipitation, size and water phase of the hydrometeors, whereas the radial velocity contains information on vertical atmospheric motions which are both important for the onset and development of convection.

During the past years, capabilities to assimilate radial velocity (Xiao et al., 2005) and reflectivity (Xiao et al., 2007; Xiao and Sun, 2007) data with the MM5/WRF three-dimensional variational data assimilation system (Barker et al., 2003, 2004; Skamarock et al., 2008) were developed at National Center for Atmospheric Research (NCAR) laboratories.

In Xiao et al. (2005) radial velocities from a single Doppler radar were assimilated into MM5 using 3DVAR scheme for a heavy rainfall case that occurred on 10 June 2002. Vertical velocity increments were included via Richardson's balance equation, and an observation operator for the radial velocity was developed. The results suggested that the scheme for radial velocity assimilation is stable and robust in a cycling mode using high-frequency radar data. Moreover, continuous assimilation with 3 h update cycles was important to improve heavy rainfall.

AMTD
6, 7315–7353, 2013

More recently, a radar reflectivity data assimilation scheme was developed within MM5-3DVAR system as described by Xiao et al. (2007). The total water mixing ratio was used as control variable for moisture and the warm rain process was incorporated into the system in order to partition the moisture and hydrometeor increments. Further, an observation operator for radar reflectivity was developed and incorporated into the 3DVAR system. They showed that the intensity and track of Typhoon Rusa (2002) were better predicted through the combined assimilation of radar radial velocity and reflectivity data.

Recently, the WRF model and its 3DVAR data assimilation system was used by Xiao and Sun (2007) to ingest data from a network of Doppler radars in order to study a squall-line convective system. They found that the combined assimilation of the radial velocity and reflectivity improved the Quantitative Precipitation Forecast (QPF) skill with respect to using only one of the two radar variables. Moreover, the assimilation of more than one radar site using cycling procedure, further improved the results in terms of QPF.

The objective of this paper is to assess the impact of the assimilation of radar radial velocity and reflectivity data on the precipitation forecast, by using 3DVAR and WRF-ARW. To this purpose, a heavy rainfall case occurred in central Italy, the Aniene event (Rome 19–22 May 2008) is used. Several numerical experiments using different ICs are performed using WRF model. To explore the impact of radar data assimilation a comparison between experiments with and without radar data is performed as well as the sensitivity to cold and warm start. Finally, to account for non linearity in the observation operators, also the role of outer loops is tested (Rizvi et al., 2008).

The novelty of this work resides in the assimilation of the radar data itself in this a complex orography area as the Mediterranean one. This was never done before, the originality of this research lie in the fact of bringing together weather forecast and radar data both still challenge in complex orography.

This paper is organized as follows. In Sect. 2, the case study and the radar data used for the assimilation are described. A brief explanation of WRF-3DVAR system

AMTD
6, 7315–7353, 2013

and radar data operator are presented in Sect. 3. The 3DVAR experiments and the corresponding forecast results are discussed in Sects. 4 and 5, respectively. The impact of non linearity is analyzed in Sect. 6, whereas summary and conclusions are provided in Sect. 7.

2 A heavy rainfall case and radar data

2.1 Case description: the Aniene event

During 19–22 May 2008 a heavy rainfall event occurred in the urban area of Rome. In the first hours of 19 May a cyclonic circulation (Fig. 1a and b) on the southern Mediterranean Sea, associated to an intrusion of cold air from Scandinavia, caused instability on the Italian peninsula. During 20 May (Fig. 1c and d) a deep cyclonic circulation developed on the Genoa Gulf, causing severe weather condition. Southwesterly flow started to blow over Tyrrhenian sea advecting warm and humid air toward the area of Rome (Fig. 1c and d) destabilizing the atmosphere.

During the evening of 20 May, as described in Sect. 2.2, the Monte Midia radar recorded reflectivity echoes with values reaching 50–55 dBZ in the north-east area of Rome, suggesting the onset of convective precipitation and echoes with reduced values of reflectivity (35–40 dBZ), more likely associated to stratiform precipitation. Thanks to its cyclonic structure, this event was interesting because it allowed analyzing both types of precipitation. The two types of echoes were registered all day long. To better understand the meteorological evolution of the event the instantaneous radiance at IR 10.8 µm and the rain rate (RR in $mm\,h^{-1}$) registered from MSG (Meteosat Second Generation) and estimated from the Italian national radar network are shown (Fig. 2). In the early afternoon the precipitation is restricted to the urban area of Rome (RM, Fig. 2a), to reach later the south-eastern part of RM with local showers (Fig. 2b). In the evening, precipitation occurred again on the urban area of RM (Fig. 2c), while at 22:00 UTC, the rainfall moved toward east close to L'Aquila (AQ, Fig. 2d).

AMTD
6, 7315–7353, 2013

2.2 Radar data processing

The GTS (Global Telecommunication System) conventional observations – SYNOP (Surface synoptic observations) and TEMP (upper level temperature, humidity and winds) – and non conventional (radar) data are used in this study. In particular, the data from Monte Midia radar (42°03′28″ N, 13°10′38″ E), provided by the Centro Funzionale of Abruzzo Region, are assimilated to improve high resolution initial conditions. This is a C band Doppler radar located at the border between the Abruzzo and Lazio regions (Fig. 3, shows the Monte Midia radar coverage and site) placed at 1710 m from the sea level, covering most of Central Italy including the Abruzzo inland and the urban area of Rome. Reflectivity and radial velocity are detected every 15 min, at 500 m horizontal resolution with four antenna elevations angles (0, 1, 2, 3°).

It is well known that radar observations can be affected by several sources of errors mainly due to ground clutter, attenuation and radio interferences. Particularly, weather radar operating in complex orography may be affected by a significant beam blockage which can strongly degrade monitoring capabilities and accordingly rainfall estimation at ground.

For such reason, a preliminary procedure to correct acquired radar data is applied, before using them into numerical models. Echoes produced by a non-meteorological source such as mountain's clutter returns, WLAN (wireless local area network) interference signals and other impairments have been removed applying a Doppler filter and a suitable texture filter. Partial beam blockage is corrected by adopting a compensating technique (Fulton et al., 1998) while attenuation is mitigated by means rain path integrated attenuation (PIA) techniques (Picciotti et al., 2006). Once corrected, radar data are ready for ingestion into 3DVAR, setting as typical error 1.0 m s^{-1} for radial velocity and 1.0 dBZ for reflectivity. The assimilation window was chosen of 5 min. The data assimilation takes place only after a quality check, in order to select only good quality data within the model domain and into the selected assimilation window.

AMTD
6, 7315–7353, 2013

3 WRF-3DVAR

3.1 Brief description of WRF-3DVAR

The WRF-3DVAR system is based on the MM5-3DVAR (Barker et al., 2004) and further developments and progresses can be referred to Skamarock et al. (2008). The configuration of the WRF-3DVAR system is based on the multivariate incremental formulation (Courtier et al., 1994): the preconditioned control variables are stream function ψ, potential velocity χ, unbalanced pressure p_u and total water mixing ratio q_t. The aim of the 3-D-Variational approach is to produce the best compromise between an a priori estimation of the analysis field and observations, through the iterative solution that minimize a cost function J. The cost function for 3DVAR is:

$$J(x) = J^b + J^0 = \frac{1}{2}\left\{\left[y^0 - H(x)\right]^T \mathbf{R}^{-1}\left[y^0 - H(x)\right] + \left(x - x^b\right)^T \mathbf{B}^{-1}\left(x - x^b\right)\right\} \quad (1)$$

where x^b is the generic variable of an a priori state (first guess), y^0 is the observation, and H is the operator that converts the model state to the observations space. This cost function J measures the distance of a field x from the observations y^0 and from the background x^b: these distances are scaled through the matrices **R** and **B**, the observational and the background error covariance matrices, respectively. **R** accounts also for representativeness and forward operator errors. The former depends on the model characteristics, whereas the latter comes from the coding of the observation operator. A good estimation of these matrices is important for producing worthwhile initial conditions. **R** is usually a diagonal well known matrix and it is assumed independent from weather conditions. On the contrary **B** is weather-condition and flow-dependent, and it also depends from the background. For these reasons, **B** has to be estimated using a statistical method, such as the National Meteorological Center (NMC) method (Parrish and Derber, 1992) or the ensemble one (Fisher et al., 1999). The first method is commonly used for the estimation of **B** in the WRF-3DVAR system. It is based on the

AMTD
6, 7315–7353, 2013

statistical analysis of several couples of forecasts differences valid at the same time. A detailed description of the 3DVAR system can be found in Barker et al. (2003, 2004).

3.2 Radar data assimilation methodology

Doppler radar data contains precious features compared to conventional observations: the radial velocity produces information on vertical motion. Although the vertical velocity is generally poorly estimated it is important for the convective onset. Moreover, it is well known that radar reflectivity is a measurement of the amount of precipitating hydrometeors (rain, snow, etc.), but due to the complexity of coding such variables, they are not included in many data assimilation schemes.

On the contrary, WRF-3DVAR has a methodology for the assimilation of Doppler radar data which accounts for both the reflectivity and vertical velocity component of radial velocity. The vertical increments are estimated including a balance equation based on Richardson (1922). This is the so-called linearized Richardson's equation, which combines continuity equation, adiabatic thermodynamic equation, and hydrostatic relation: it becomes important when radar data are included in the analysis and for small scale convective weather systems.

Moreover, the total water q_t is used as the moisture control variable, instead of the pseudo relative humidity, for the assimilation of radar reflectivity (Xiao et al., 2007).

3.2.1 Assimilation of reflectivity

To directly assimilate radar reflectivity, the total water mixing ratio q_t was chosen as control variable, and a warm rain process to divide the moisture, q_v, and water hydrometeor, q_c and q_r, contributions was introduced (Dudhia, 1989) into the WRF-3DVAR system. This allowed for producing the increments of moist variables linked to the hydrometeors, such as water vapor mixing ratio q_v, cloud water mixing ratio q_c, and rainwater mixing ratio q_r. Once the 3DVAR system produces the q_c and q_r increments, the setup of the observation operator for assimilation of reflectivity is straightforward.

AMTD
6, 7315–7353, 2013

In this study, the operator from Sun and Crook (1997) is used:

$$Z = 43.1 + 17.5 \log(\rho q_r) \quad (2)$$

where Z is the radar reflectivity in the unit of dBZ, ρ the air density (kg m^{-3}) and q_r is the rain water mixing ratio (g kg^{-1}). This relation was derived analytically by assuming the Marshall–Palmer distribution of raindrop size with intercept $N_0 = 8 \times 10^6$ mm^{-4} and no contribution of ice phases to the reflectivity.

Efforts to improve the rain radar estimation have been made for Monte Midia radar. This was accomplished by comparing rain retrieved by radar to rain recorded by rain gauge and searching for the best estimation which minimizes the error between the two rain values (Picciotti et al., 2010). This procedure was carried out accounting for a large data set covering two years, carefully collected and processed. This allowed for correcting Eq. (2) to better represent the Monte Midia rain estimates as follows:

$$Z = 7.27 + 33.8 \log(\rho q_r). \quad (3)$$

3.2.2 Assimilation of radial velocities

The observation operator for Doppler radial velocity is:

$$V_r = u\frac{x - x_i}{r_i} + v\frac{y - y_i}{r_i} + (w - v_t)\frac{z - z_i}{r_i} \quad (4)$$

here (u, v, w) are the wind components; (x, y, z) are the radar site components; (x_i, y_i, z_i) are components of the radar observation; r_i is the distance between the radar site and the observation; v_t is the terminal velocity.

Following the algorithm of Sun and Crook (1998) the terminal velocity is given by:

$$v_t = 5.40a \cdot q_r^{0.125} \quad (5)$$

where "a" is a correction factor defined as follow:

$$a = \left(p_0/\bar{p}\right)^{0.4} \quad (6)$$

where $\bar{p}$ is the base-state pressure and p_0 is the pressure at the ground.

AMTD
6, 7315–7353, 2013

4 Experiments configuration

4.1 Model setup

The Weather Research and Forecasting model version 3.2 (Wang et al., 2011) is used for this study.

Three two-way nested domains (D*i*) centered over the area where high precipitation occurred (Fig. 4), with a resolution in km of 21.2 (D1), 7.06 (D2) and 2.35 (D3) respectively and 37 vertical levels are used.

All of the physical parameterizations in our experiments are the same, which include WRF Single-Moment 6-class (Hong and Lim, 2006) explicit microphysical scheme, the Kain–Fritsch (2004) for the cumulus convection, for D1 and D2 only, the Yonsey University scheme (Hong et al., 2006) for the Planetary Boundary Layer, Rapide Radiative Transfer Model (Mlawer et al., 1997) and Dudhia (1989) schemes for longwave and shortwave radiation respectively.

4.2 WRF-3DVAR setup

To the aim of investigating the impact of radar data on the model precipitation, several Initial Conditions (ICs) using different assimilation strategies are produced for WRF using 3DVAR. Besides the first guess x^b and observations y^0, as explained in the Sect. 3.1, another important input for WRF-3DVAR is the background error covariance matrix **B**, computed using NMC-method which accounts for ECMWF data on Mediterranean Basin. To estimate the NMC-based error statistics, two forecasts have been performed every day for a period of 4 weeks, starting on 15 May 2008: a 24 h forecast (starting from 00:00 UTC) and a 12 h forecast (starting from 12:00 UTC). The differences between the two forecasts at $t+24$ and $t+12$ respectively are used to calculate the domain-averaged error statistics.

AMTD
6, 7315–7353, 2013

4.3 Experimental design

A total of four WRF experiments are performed using the ICs produced by the WRF-3DVAR system: the control experiment (Exp0) is initialized using ECMWF analysis (0.25° × 0.25°) and no data assimilation is performed; Exp1 is as Exp0, but the assimilation of Monte Midia radar data (both reflectivity and radial velocity) using a specific **B** calculated for each domain is performed; a warm start from a previous 24 h WRF forecast and assimilation of both conventional data and radar data is used for Exp2; Exp3 is initialized using a 3 h WRF forecast cycle (Fig. 5) with assimilation of both conventional data and radar data from 00:00 to 06:00 UTC 20 May 2008. For both Exp2 and Exp3 a specific background error covariance matrix calculated for each domain is used. Data assimilation is performed on each domain and one outer loop is used as default.

All experiments last 24 h, from 06:00 UTC 20 May 2008 until 06:00 UTC 21 May. They are summarized in Table 1.

5 Numerical results

5.1 Initial conditions

To evaluate the impact of 3DVAR on the Initial Conditions a comparison between the vertical sounding produced by 3DVAR and the observed one at Pratica di Mare (PDM) at 06:00 UTC 20 May 2008 is performed. The comparison is carried out using a few meteorological indexes as: Convective Available Potential Energy (CAPE), useful for assessing the instability of the atmosphere and therefore the possibility of triggering convection; Lifted Index (LI), that measure the severity of the thunderstorm; K-index (KINX), that gives an indication on the thunderstorm occurrence. Large differences are found among the experiments except for the KINX as listed in Table 2.

AMTD
6, 7315–7353, 2013

A large underestimation of CAPE for most of the experiments is found except for Exp3, which produces a value closer to the observed one than the other experiments, whereas LI is overestimated, but still in the range of a weak chance of severe thunderstorm. Finally, KINX is pretty the same for all the experiments, inferring that all of them produce a thundery atmosphere. These results would suggest that the warm start 3 h cycling used for this experiment slightly increases the potential for thunderstorm development.

The observed (Fig. 6) and the WRF-3DVAR radio sounding at Pratica Di Mare at 06:00 UTC 20 May 2008 clearly show (Fig. 7) no differences among Exp0, 1 and 2, but differences are found with respect to the observed one especially between 850 and 700 hPa. Exp3 (Fig. 7d) shows higher moisture content below 700 hPa than the other experiments (Fig. 7a–c) increasing the agreement with the observed one (Fig. 6). This higher moisture content justifies the higher K-index and atmospheric instability. These support the more unstable atmosphere as indicated by the convective indices. Finally, the wind does not show any difference among the experiments (Fig. 7) and a fair agreement for all of them with the observed one (Fig. 6).

5.2 WRF vs. radar reflectivity and rainfall

The impact of Monte Midia radar data assimilation on the forecast is evaluated by comparing the observed reflectivity and estimated rain rate with those produced by the WRF experiments.

Impact of ICs' on WRF forecast

The radar detected reflectivity of approximately 50–55 dBZ at 14:00 UTC associated to a few small intense convective cells north-south oriented between Rome (RM) and Rieti (RI) (solid red oval in Fig. 8). Another area of moderate precipitation (about 40 dBZ) between the border of Lazio and Abruzzo (red arrow in Fig. 8) was also detected. Most of the WRF experiments succeed in reproducing the cells orientation, except for Exp3,

AMTD
6, 7315–7353, 2013

but an underestimation is found (Fig. 9). Exp0 underestimate the number of cells in the red circle (Fig. 9, top left panel), but correctly reproduces their intensity. On the contrary, Exp0 overestimates the cells along the boundaries (Fig. 9, top left panel, red arrow), both in intensity and size. Similarly Exp1 overestimates the intensity and the size of the cells indicated by the red arrow (Fig. 9, top right panel). Moreover, the size and the intensity of the cells inside the red circle is overestimated (Fig. 9, top right panel). Exp2 shows a different cells distribution inside the red circle, but with the same intensity as Exp0 (Fig. 9, bottom left panel), whereas an overestimation in size and intensity of the radar reflectivity in the area indicated by the red arrow is found. Exp3 does not reproduce any cell inside the red circle, but correctly reproduces the size and the intensity of the cells along the boundaries between Lazio and Abruzzo. These results suggest that WRF enhances convection, especially when data assimilation and warm start are performed as for Exp2, but the 3 h cycling strongly impacts the dynamic of the cyclone, changing the timing of occurrence and the intensity of convection.

Similarly to the reflectivity, a comparison between the observed and the WRF 12 h accumulated rainfall is now performed. The 12 h accumulated precipitation ending at 22:00 UTC on 20 May 2008 clearly shows (Figs. 10 and 11) that, beside a correct maximum amount the first three experiments produce a rainfall areal distribution barely comparable to the observed. On the contrary, Exp3 (Fig. 11, bottom right panel) overestimates the precipitation but well reproduces rainfall pattern except for the precipitation on the northwestern side of Rome. In fact, the precipitation both on northeast and east of Frosinone (FR, Fig. 11, bottom right panel) is fairly reproduced as well as an attempt to reproduce the signal of almost no precipitation on the left side of the Apennine increasing again along the east coast (Figs. 10 and 11, bottom right panels).

Therefore, the previous results would suggest Exp3 as the only one able to reproduce this event.

AMTD
6, 7315–7353, 2013

5.3 Effects on some statistical indicators

In order to objectively compare the experiments carried out for the Aniene event, four statistical indicators are used (Wilks, 1995): forecast accuracy (ACC), false alarm rate (FAR), frequency bias (FBIAS) and equitable threat score (EQTS). The forecast evaluation is performed using rain gauges data, coming from the stations of the Lazio region (Fig. 12, yellow dots), providing 12 h accumulated precipitation. Figure 12 shows also the Aniene basin (green line) and the total amount of interpolated precipitation registered for the entire event 19–22 May 2008.

The ACC index shows the accuracy of the forecast, a perfect forecast has ACC = 1; FAR estimates the forecast frequency failures, a perfect forecast has FAR = 0; FBIAS gives information on the correctness of the precipitation forecast: values greater than 1 indicates an overestimation in the number of forecast events, the perfect value is FBIAS = 1; EQTS, whose best value is 1, represents the fraction of the events correctly reproduced taking into account random hit chance; the EQTS index may have values lower than or near zero if the forecasts are wrong so values of 0.5/0.6 are considered fairly good.

Figure 13 shows the results for the previous indices for the 12 h accumulated rainfall ending at 04:00 UTC 21 May 2008 as a function of different thresholds. ACC, FBIAS and EQTS display the best values for Exp3 (Fig. 13, pink line) for thresholds lower than approximately 20 mm h^{-1}, whereas for higher thresholds only Exp2 (Fig. 13, green curve) produces results better than the others, especially for EQTS. It is well known that a good EQTS may be associated to an overestimation of the precipitation. In fact, Exp3 has the worst FAR for almost all thresholds. These results would support the previous finding that the experiment performed using the ICs produced by a warm start using a 3 h cycle improve the forecast.

AMTD
6, 7315–7353, 2013

6 Impact of multiple outer loops strategy

Based on the previous results, a set of sensitivity tests for WRF-3DVAR are performed for Exp1, Exp2 and Exp3. These new experiments are carried out using 2 and 3 outer loops during the assimilation procedure (Table 3). Multiple outer loops strategy allows for including the non-linearity in the observation operators and for assessing the influence of observations entering for each cycle.

Figure 14 shows the impact of the outer loops on the reflectivity for Exp1. Clearly, the overestimation of the line of convective cells on 20 May (Fig. 9, right top panel, to compare with red circle on Fig. 8) is largely reduced turning into a better reproduced structure: three single cells north-south aligned are now produced by using multiple outer loops for Exp1_2OL (Fig. 14, left panel).

If three outer loops are used the convection completely disappear.

For Exp2 the positive impact of multiple outer loops is clearly visible once again for the convective line between RM and RI if using 2 outer loops (Fig. 15, Exp2_2OL). Also in this case the three loops deteriorate the results but in the opposite direction with respect to Exp1. In fact, in this case an overestimation of the reflectivity in the area between Rieti and Roma is found (Fig. 15, right panel).

Finally, a quite different impact is obtained for Exp3 (Fig. 16); the line of convective cells starts forming especially when 3 outer loops are used, even if their intensity is not comparable to the observed one (Fig. 8, red circle).

To better evaluate the impact of outer loops ACC, FAR, FBIAS and EQTS are used. Only the results for Exp2 are shown. If 2 outer loops are used during the assimilation process better scores (Fig. 17, red curve) are obtained, especially for thresholds lower than $20\,\mathrm{mm\,h^{-1}}$ and for EQTS index once compared with blue curve (1 loop). On the contrary, for higher thresholds ($30\,\mathrm{mm\,h^{-1}}$) positive results for the EQTS and FAR (green curve, Fig. 17, bottom panel) are obtained if using 3 outer loops.

AMTD
6, 7315–7353, 2013

7 Summary and conclusions

A heavy rainfall event in the urban area of Rome is used to investigate the impact of assimilation of radar data on the WRF forecast. In order to provide model Initial Conditions with high-resolution information, radar radial velocity and reflectivity data are assimilated using the WRF-3DVAR scheme. Several forecast experiments, including cold start and warm start, sensitivity tests to a different assimilation strategy and to multiple outer loops, to assess the impact of radar data assimilation are performed.

Major conclusions are summarized as follows:

- the warm start experiment (Exp2) clearly shows an improved forecast with respect to the cold start experiments (Exp1);
- "3 h-DA cycle" assimilation strategy (Exp3) produces improved forecast although it needs more accurate analysis;
- the outer loops strategy allows assimilation of a larger number of observations, in fact by increasing the outer loop iterations, more observations are getting assimilated into WRF-3DVAR; this turns into a forecast improvement, especially for very localized cells as for Exp2.

In conclusion, the assimilation of radar radial velocity and reflectivity data seems to have a positive impact on the forecast of precipitation, especially when they are ingested together with conventional observations and warm start (or cycling) is used. This is because the cycling benefits from the information transfer of the previous forecast. However, the cycling should be used with caution because the analysis can include noise and imbalances.

Finally, three important limitations that have certainly influenced the results are: (1) the lack of the ice phase in the 3DVAR microphysics, (2) computation of **B** matrix could be improved by using the ensemble forecasts or the Ensemble Kalman Filter, (3) the absence of radar observations on the Tyrrhenian coastline from where the system approaches.

AMTD
6, 7315–7353, 2013

Moreover, the technique of multiple outer loops should be further investigated with different background error statistics tuning, but unfortunately each extra outer loop is equivalent to one analysis run in term of execution time. Also thinning of radar data has to be undertaken either to reduce the observation-error spatial correlation or to reduce the computational cost of the assimilation (Montmerle and Faccani, 2009).

For the next future we are exploring the possibility of extending the radar assimilation procedure using data from several operative radars located on Central Italy, including also dual-polarization systems.

Acknowledgements. The authors are grateful to HIMET (High Innovation in Meteorology and Environmental Technologies) and Sapienza University of Rome for radar and computing resources support, as well as the National Department for Civil Protection. NCAR is also acknowledged for WRF and 3DVAR system.

References

Barker, D. M., Huang, W., Guo, Y.-G., and Bourgeois, A.: A Three-Dimensional Variational (3DVAR) Data Assimilation System For Use With MM5, NCAR Tech. Note, NCAR/TN-453+STR, UCAR Communications, Boulder, CO, 68 pp., 2003.

Barker, D. M., Huang, W., Guo, Y.-R., Bourgeois, A., and Xiao, Q.: A Three-Dimensional Variational (3DVAR) data assimilation system for use with MM5: implementation and initial results, Mon. Weather Rev., 132, 897–914, 2004.

Courtier, P., Thépaut, J.-N., and Hollingsworth, A.: A Strategy for Operational Implementation of 4D-Var Using an Incremental Approach, Q. J. Roy. Meteorol. Soc., 120, 1367–1387, 1994.

Dudhia, J.: Numerical study of convection observed during the winter monsoon experiment using a mesoscale two-dimensionale model, J. Atmos. Sci., 46, 3077–3107, 1989.

Fisher, M.: Background Error Statistics Derived from en Ensemble of Analysis, ECMWF Research Department Technical Memorandum, 79, ECMWF, Shinfield Park, Reading, UK, 12 pp., 1999.

Fulton, R. A., Breidenbach, J. P., Seo, D., Miller, D., and O'Bannon, T.: The WSR-88D rainfall algorithm, Weather Forecast., 13, 377–395, 1998.

AMTD
6, 7315–7353, 2013

Hong, S. Y. and Lim, J.-O. J.: The WRF single-moment 6-class microphysics scheme (WSM6), J. Korean Meteorol. Soc., 42, 129–151, 2006.
Hong, S. Y., Ying, N., and Dudhia, J.: A new vertical diffusion package with an explicit treatment of entrainment processes, Mon. Weather Rev., 134, 2318–2341, 2006.
Kain, J. S.: The Kain–Fritsch convective parameterization: an update, J. Appl. Meteorol., 43, 170–181, 2004.
Kalnay, E.: Atmospheric Modeling, Data Assimilation and Predictability, Cambridge University Press, Cambridge, UK, 364 pp., 2003.
Mlawer, E. J., Taubman, S. J., Brown, P. D., Iacono, M. J., and Clough, S. A.: Radiative transfer for inhomogeneous atmosphere: RRTM, a validated correlated-*k* model for the long-wave, J. Geophys. Res., 102, 16663–16682, 1997.
Montmerle, T. and Faccani, C.: Mesoscale assimilation of radial velocities from Doppler radars in a preoperational framework, Mon. Weather Rev., 137, 1939–1953, 2009.
Parrish, D. F. and Derber, J. C.: The National Meteorological Center's spectral statistical-interpolation analysis system, Mon. Weather Rev., 120, 1747–1763, 1992.
Picciotti, E., Montopoli, M., Gallese, B., Cimoroni, A., Ferrauto, G., Ronzitti, L., Mancini, G., Volpi, A., Sabatini, F., Bernardini, L., and Marzano, F. S.: Rainfall Mapping in Complex Orography from C-band RADAR at Mt. Midia in Central Italy: Data Synergy and Adaptive Algorithms, Proceeding of ERAD 2006, Barcelona, Spain, 341–344, 2006.
Picciotti, E., Montopoli, M., Di Fabio, S., and Marzano, F. S.: Statistical Calibration of Surface Rain Fields from C-band Mt. Midia Operational RADAR in Central Italy, ERAD 2010, Sibiu, Romania, 2010.
Richardson, L. F.: Weather Prediction by Numerical Process, Cambridge University Press, Cambridge, UK, 236 pp., 1922.
Rizvi, S., Guo, Y.-R., Shao, H., Demirtas, M., and Huang, X.-Y.: Impact of outer loop for WRF data assimilation system (WRFDA), 9th WRF Users' Workshop, 23–27 June 2008, Boulder, Colorado, 2008.
Skamarock, W. C., Klemp, J. B., Dudhia, J., Gill, D. O., Barker, D. M., Duda, M. G., Huang, X.-Y., Wang, W., and Powers, J. G.: A description of the Advanced Reasearch WRF Version 3, NCAR Technical Note, TN 475+STR, 113 pp., available from http://www.mmm.ucar.edu/wrf/users/docs/arw_v3.pdf (last access: January 2012), 2008.

AMTD
6, 7315–7353, 2013

Sun, J. and Crook, N. A.: Dynamical and microphysical retrieval from Doppler RADAR observations using a cloud model and its adjoint, Part I: model development and simulated data experiments, J. Atmos. Sci., 54, 1642–1661, 1997.

Sun, J. and Crook, N. A.: Dynamical and microphysical retrieval from Doppler RADAR observations using a cloud model and its adjoint, Part II: Retrieval experiments of an observed Florida convective storm, J. Atmos. Sci., 55, 835–852, 1998.

Wang, W., Bruyère, C., Duda, M., Dudhia, J., Gill, D., Lin, H.-C., Michalakes, J., Rizvi, S., Zhang, X., Beezley, J. D., Coen, J. L., and Mandel, J.: ARW, Version 3 Modeling System User's Guide, Mesoscale and Microscale Meteorology Division, National Center for Atmospheric Research, available online at http://www.mmm.ucar.edu/wrf/users/docs/user_guide_V3/ARWUsersGuideV3.pdf, last access: April 2011.

Wilks, D. S.: Statistical Methods in the Atmospheric Sciences, Academic Press, San Diego, USA, 467 pp., 1995.

Xiao, Q. and Sun, J.: Multiple-RADAR data assimilation and short-range quantitative precipitation forecasting of a squall line observed during IHOP_2002, Mon. Weather Rev., 135, 3381–3404, 2007.

Xiao, Q., Kuo, Y.-H., Sun, J., and Lee, W.-C.: Assimilation of Doppler RADAR observations with a regional 3DVAR system: impact of Doppler velocities on forecasts of a heavy rainfall case, J. Appl. Meteorol., 44, 768–788, 2005.

Xiao, Q., Kuo, Y.-H., Sun, J., Chaulee, W., and Barker, D. M.: An approach of RADAR reflectivity data assimilation and its assessment with the inland QPF of Typhoon Rusa (2002) at landfall, J. Appl. Meteorol. Clim., 46, 14–22, 2007.

AMTD
6, 7315–7353, 2013

Table 1. Description of the WRF experiments.

Exp0	initialized using ECMWF analysis and no data assimilation
Exp1	cold start with radar data assimilation, using ECMWF analysis as FG
Exp2	warm start with assimilation of both conventional and radar data, using a previous WRF forecast lasting 24 h as FG
Exp3	warm start obtained from a 3 h-DA cycle, with assimilation of both conventional and radar data, using a 3 h WRF forecast cycle as FG

AMTD
6, 7315–7353, 2013

Table 2. Values of CAPE, LI, and KINX indexes for PDM sounding and those produced by model at the same time and location.

	PDM	Exp0	Exp1	Exp2	Exp3
CAPE ($J kg^{-1}$)	193.18	79	76	76	214
LI (°C)	−0.28	−0.4	−0.4	−0.4	−1.4
KINX (°C)	31.30	30	30	30	31

AMTD
6, 7315–7353, 2013

Table 3. Description of the experiments performed using 3DVAR with multiple outer loops.

Exp1_2OL	As Exp1, setting 2 outer loops	Exp1_3OL	As Exp1, setting 3 outer loops
Exp2_2OL	As Exp2, setting 2 outer loops	Exp2_3OL	As Exp2, setting 3 outer loops
Exp3_2OL	As Exp3, setting 2 outer loops	Exp3_3OL	As Exp3, setting 3 outer loops

AMTD
6, 7315–7353, 2013

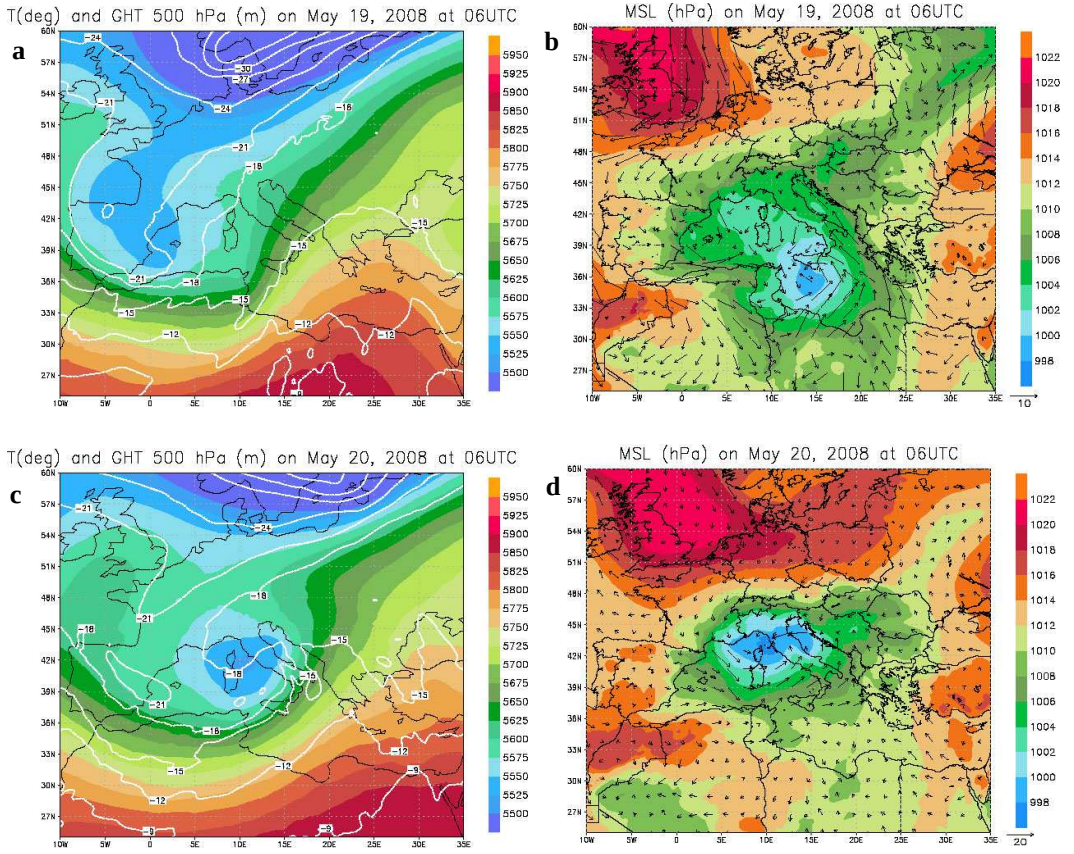

Fig. 1. ECMWF analyses at 06:00 UTC on 19 May 2008: **(a)** temperature and geopotential height, at 500 hPa, **(b)** mean sea level pressure and surface wind; ECMWF analyses at 06:00 UTC on 20 May 2008: **(c)** temperature and geopotential height, at 500 hPa, **(d)** mean sea level pressure and surface wind.

AMTD
6, 7315–7353, 2013

Impact of radar data assimilation using WRF 3-D variational system

I. Maiello et al.

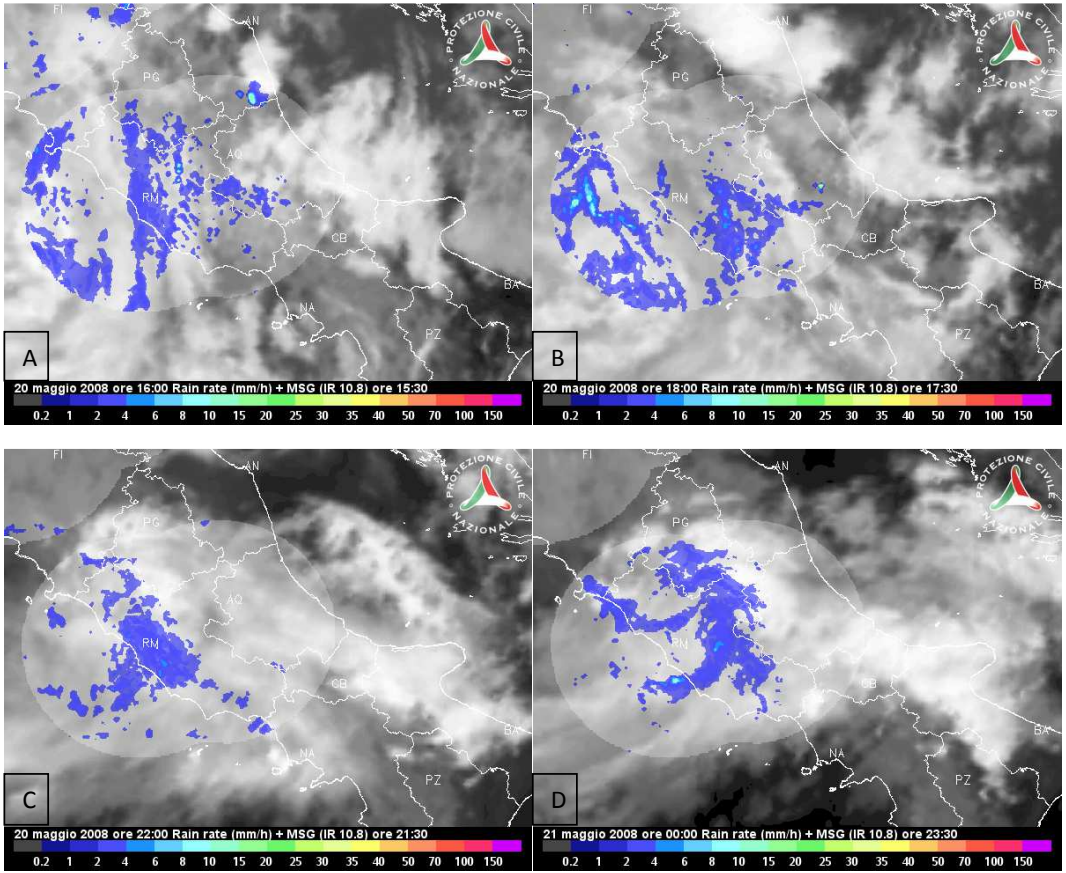

Fig. 2. MSG IR 10.8 µm and national radar network estimated rain rate ($mm\,h^{-1}$) images on Central Italy during 20 May: **(A)** RR at 14:00 UTC + MSG at 13:30 UTC; **(B)** RR at 16:00 UTC + MSG at 15:30 UTC; **(C)** RR at 20:00 UTC + MSG at 19:30 UTC; **(D)** RR at 22:00 UTC 20 May + MSG at 21:30 UTC.

AMTD
6, 7315–7353, 2013

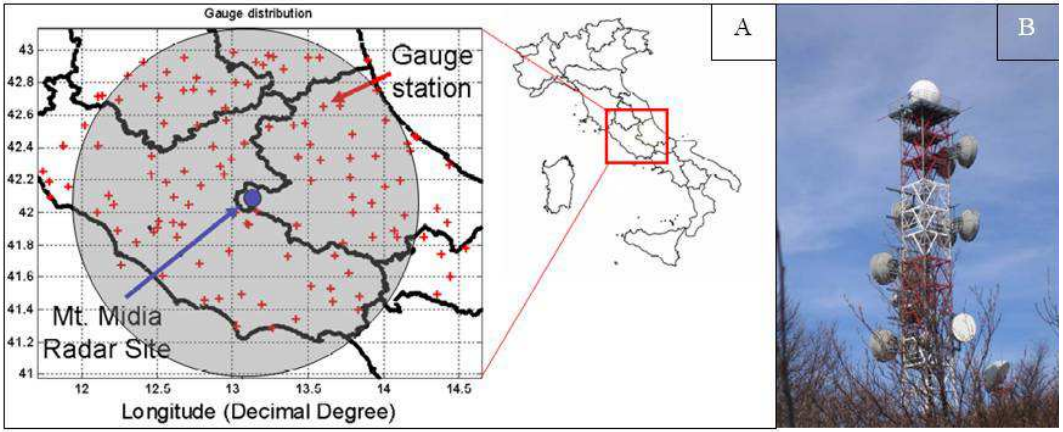

Fig. 3. Monte Midia radar site. **(A)** shows the location between the Abruzzo (to the right) and Lazio (to the left) regions, radar coverage (gray circle) and rain gauges network (red plus) used for its calibration, whereas **(B)** shows radar antenna on the top of 50 m height tower.

AMTD
6, 7315–7353, 2013

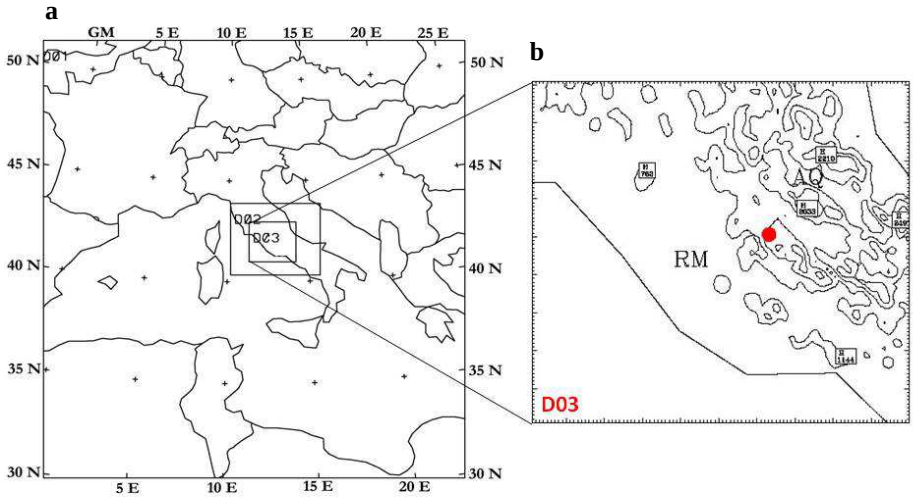

Fig. 4. Model configuration for WRF-ARW simulations using three two-way nested domains: **(a)** coarse resolution domain D01 with $\Delta x = 21.2$ km; **(b)** the high resolution D03 ($\Delta x = 2.35$ km), centered where high precipitation occurred, includes Monte Midia radar (red dot in the figure). Topography contour interval = 500 m.

AMTD
6, 7315–7353, 2013

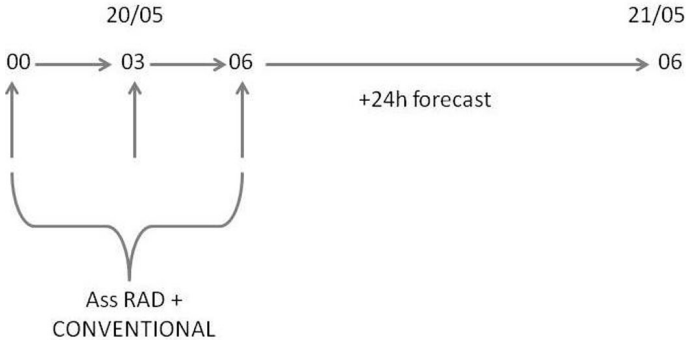

Fig. 5. Scheme for 3 h cycling procedure adopted for Exp3: in the six hours before the forecast start time (06:00 UTC 20 May), assimilation of both radar and conventional observations is performed every 3 h.

AMTD
6, 7315–7353, 2013

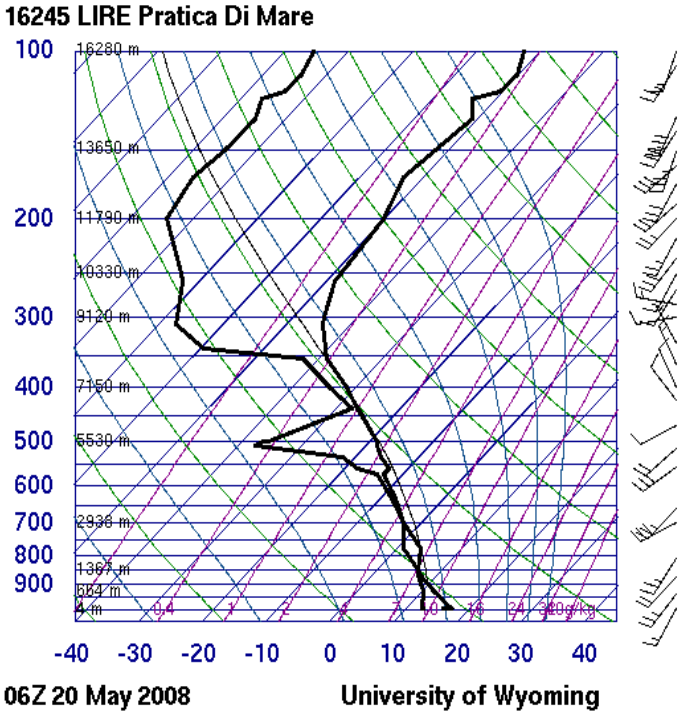

Fig. 6. PDM sounding at 06:00 UTC 20 May 2008.

AMTD
6, 7315–7353, 2013

Impact of radar data assimilation using WRF 3-D variational system

I. Maiello et al.

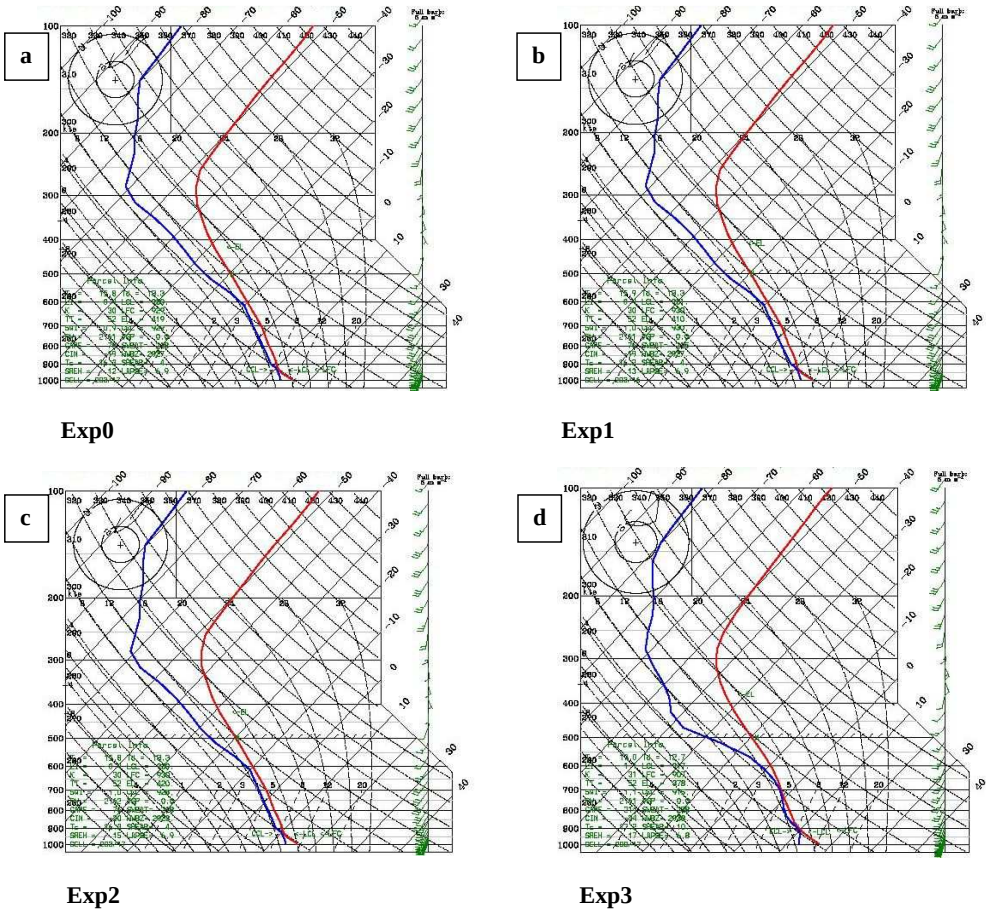

Fig. 7. WRF sounding at 06:00 UTC 20 May 2008 at PDM for: **(a)** Exp0; **(b)** Exp1; **(c)** Exp2; **(d)** Exp3.

AMTD
6, 7315–7353, 2013

Impact of radar data assimilation using WRF 3-D variational system

I. Maiello et al.

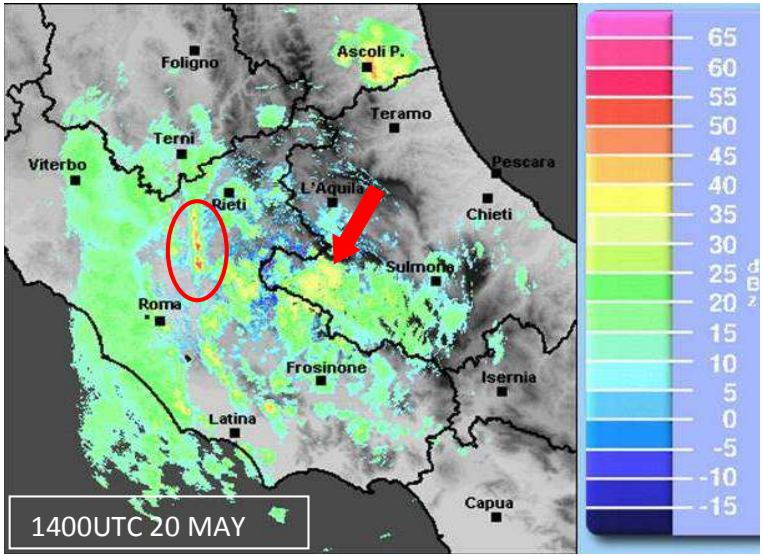

Fig. 8. Monte Midia radar reflectivity at 14:00 UTC 20 May 2008. The solid red circle and the red arrows indicate the precipitation patterns selected for the analysis.

AMTD
6, 7315–7353, 2013

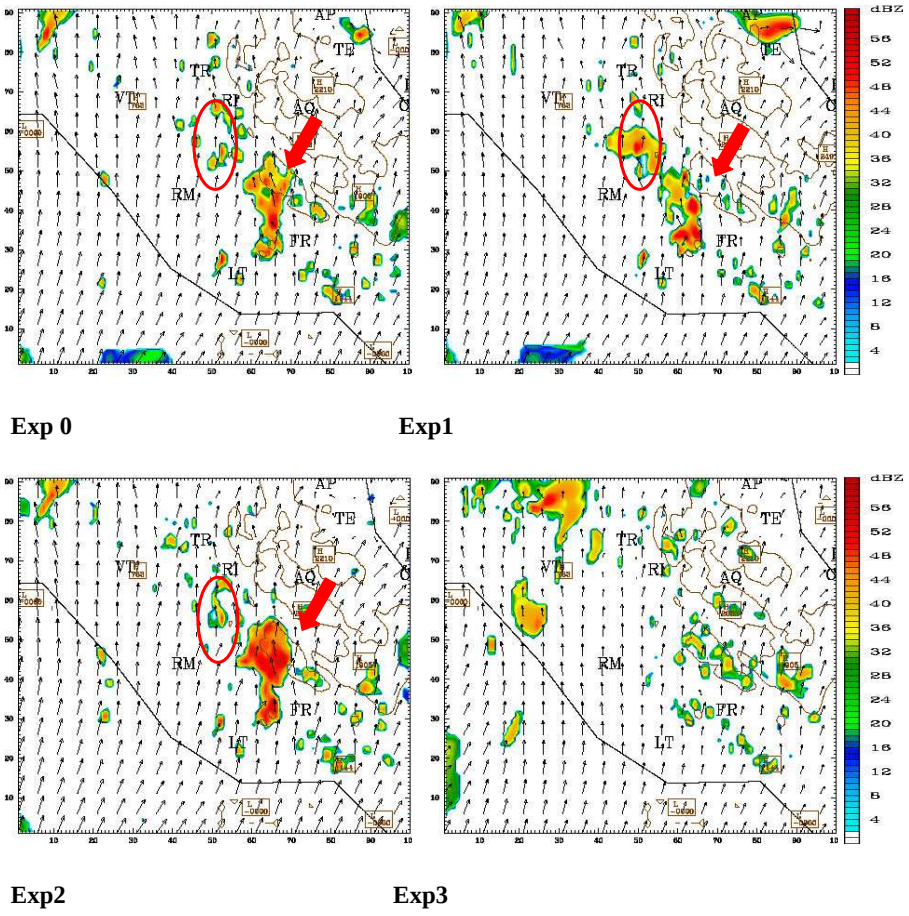

Fig. 9. WRF Reflectivity at 14:00 UTC on 20 May 2008 for experiments Exp0, Exp1, Exp2 and Exp3.

AMTD
6, 7315–7353, 2013

Impact of radar data assimilation using WRF 3-D variational system

I. Maiello et al.

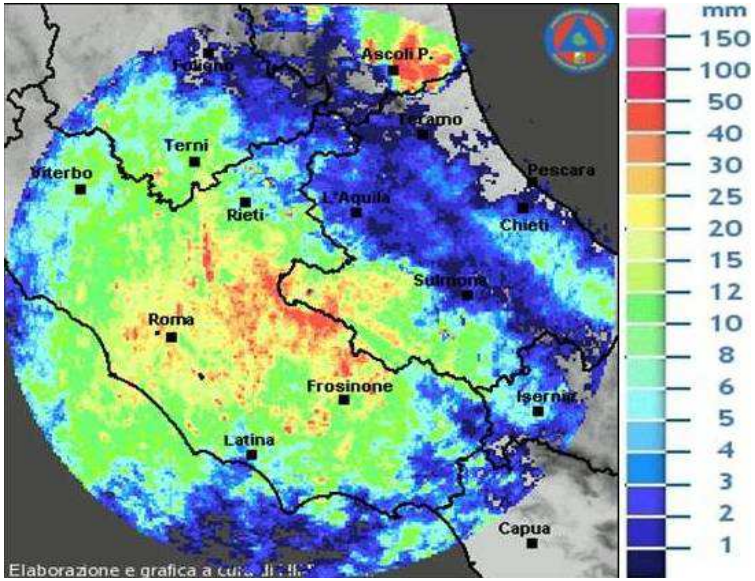

Fig. 10. 12 h accumulated rainfall ending at 22:00 UTC 20 May 2008 estimated by radar.

AMTD
6, 7315–7353, 2013

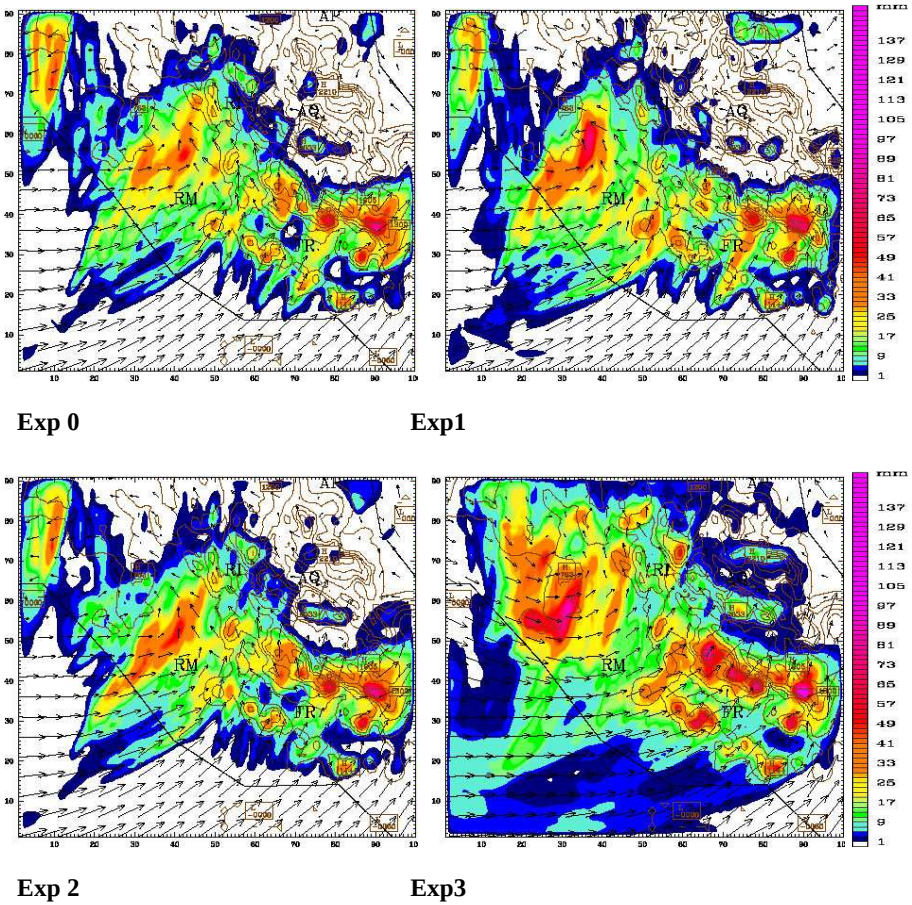

Fig. 11. 12 h accumulated rainfall ending at 22:00 UTC 20 May 2008 estimated by WRF experiments Exp0, Exp1, Exp2 and Exp3.

AMTD
6, 7315–7353, 2013

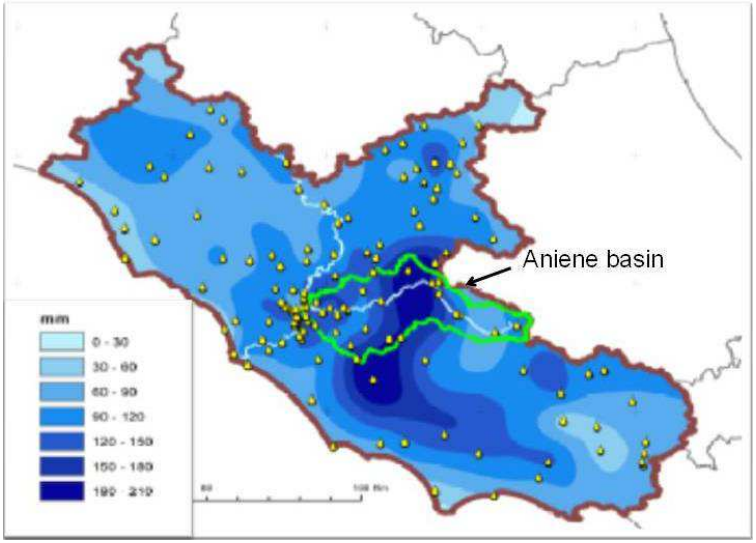

Fig. 12. Map of rain gauges stations over Lazio region (yellow dots), contour of the Aniene basin (green line) and total accumulated rainfall for the period 19–22 May 2008 (Courtesy of: Centro Funzionale of Lazio Region).

AMTD
6, 7315–7353, 2013

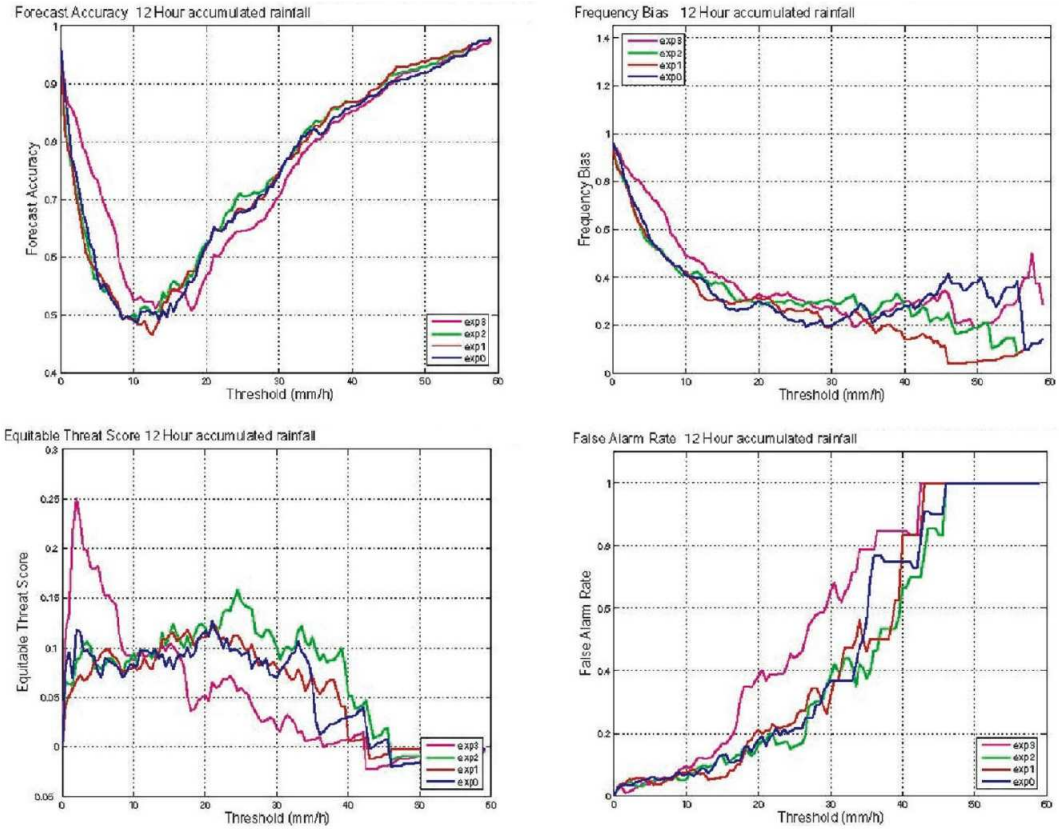

Fig. 13. ACC (top left panel), FBIAS (top right panel), EQTS (bottom left panel) and FAR (bottom right panel) used for the objective analysis of the four experiments as a function of threshold. The color code is: Exp0 blue line, Exp1 red line, Exp2 green line, Exp3 pink line. Rainfall ending at 04:00 UTC 21 May 2008.

AMTD
6, 7315–7353, 2013

Impact of radar data assimilation using WRF 3-D variational system

I. Maiello et al.

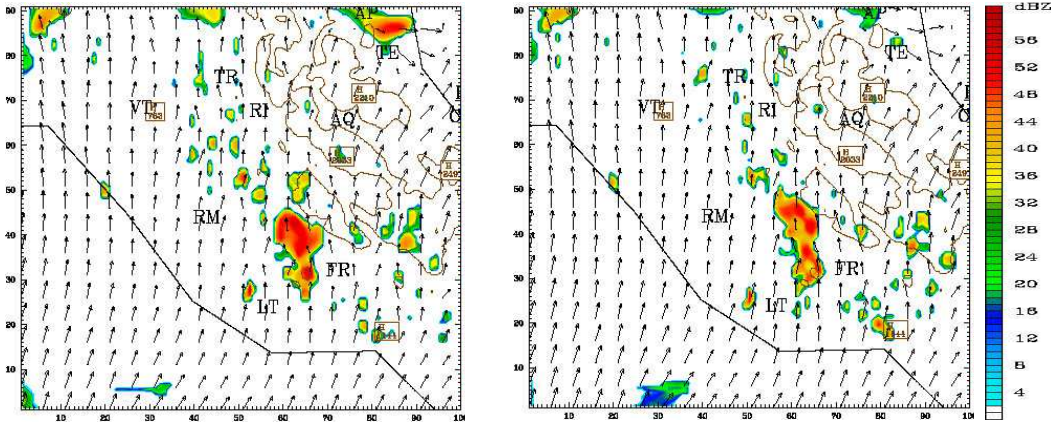

Exp1_2OL **Exp1_3OL**

Fig. 14. Reflectivity simulated by the experiment Exp1 with 2 and 3 outer loops at 14:00 UTC 20 May 2008.

AMTD
6, 7315–7353, 2013

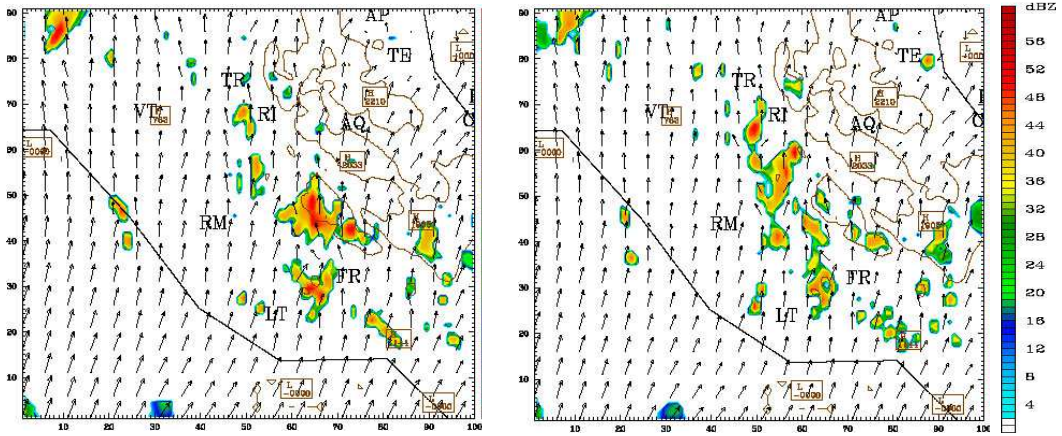

Exp2_2OL **Exp2_3OL**

Fig. 15. Reflectivity simulated by the experiment Exp2 with 2 and 3 outer loops at 14:00 UTC 20 May 2008.

AMTD
6, 7315–7353, 2013

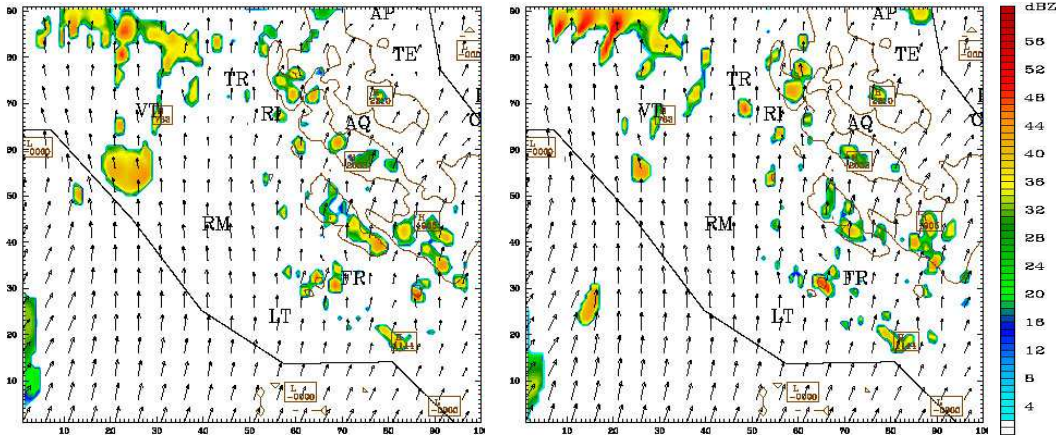

Exp3_2OL **Exp3_3OL**

Fig. 16. Reflectivity simulated by the experiment Exp3 with 2 and 3 outer loops at 14:00 UTC 20 May 2008.

AMTD
6, 7315–7353, 2013


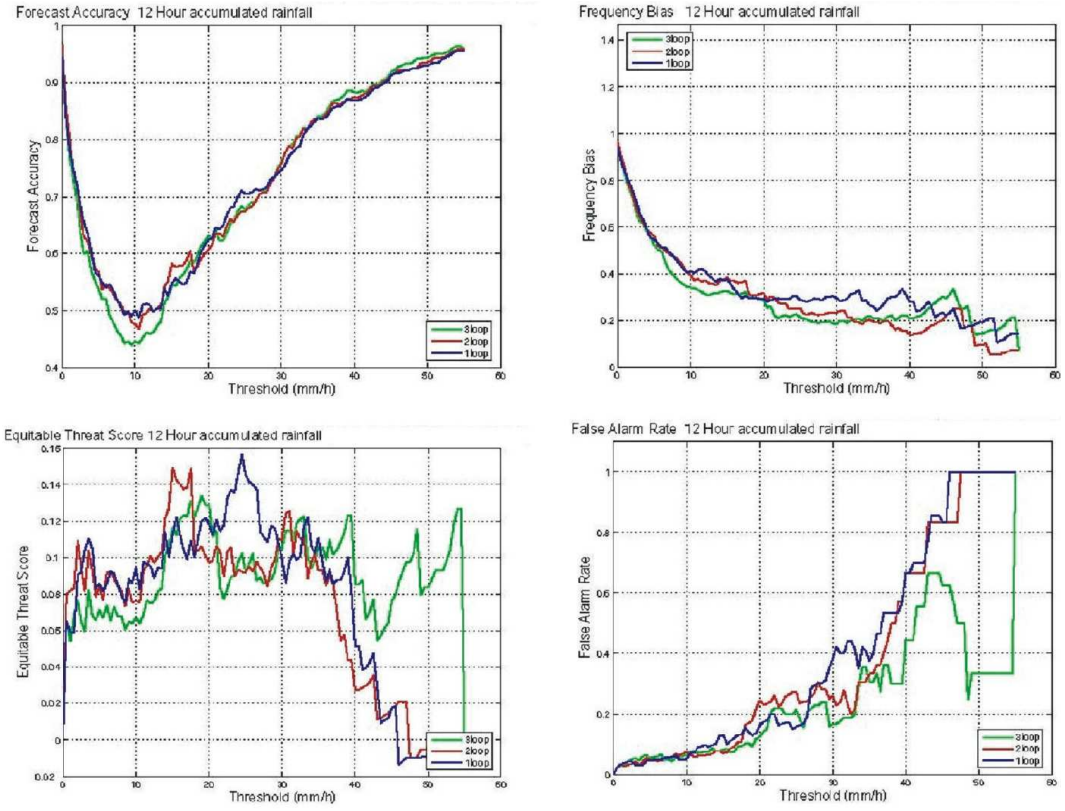

Fig. 17. ACC, FBIAS, EQTS and FAR for Exp2 about outer loops sensitivity: 1 loop green line; 2 loop red line; 3 loop blue line. Rainfall ending at 04:00 UTC 21 May 2008.

AMTD
6, 7315–7353, 2013